12. METAMORPHIC PROCESSES IN SEDIMENTS IN CONTACT WITH YOUNG OCEANIC CRUST—EAST PACIFIC RISE, LEG 65[1]

C. Rangin, Département de Géologie Structurale, Université Pierre et Marie Curie, 75230 Paris Cédex 05, France
A. Desprairies, Laboratoire de Geochimie des Roches Sédimentaires,
J. C. Fontes, Laboratoire d'Hydrologie et de Géologie Isotopique, Université de Paris-Sud, 91405 Orsay, France
C. Jehanno, Centre des Faibles Radioactivés, Laboratoire CEA/CNRS, 91190 Gif-Sur-Yvette, France
and
S. Vernhet, ERA 765 CNRS, Laboratoire de Géochimie des Roches Sédimentaires,
Université de Paris-Sud, 91405 Orsay, France

INTRODUCTION

Sites 482, 483, and 485 were drilled during Leg 65 on young oceanic crust south of the Tamayo Transform Fault. The Leg 65 drilling program was part of a multinational effort to study the East Pacific Rise (EPR) and complements sea bottom surveys conducted both in this area (Lewis, 1979; Cyamex Scientific Team and Pastouret, 1981) and farther south at 21°N (Larson, 1971; Normark, 1976; Cyamex Scientific Team; Rise Project Group, 1980). These studies, which included deep-tow, Angus and submersible surveys, were recently complemented by sea-beam surveys conducted by the *Jean Charcot* on the Tamayo Fracture Zone and farther south along the EPR. They have led to a better understanding of the magmatic, tectonic, and sedimentary processes occurring on the East Pacific Rise between the Tamayo and Rivera fracture zones.

The purpose of this chapter is to describe the metamorphic processes affecting Pliocene through Quaternary sediments found in contact, or interlayered, with basaltic units drilled during Leg 65 at the mouth of the Gulf of California.

GEOLOGIC SETTING

The sediments in the mouth of the Gulf of California were deposited at relatively high sedimentation rates and are largely hemipelagic. Their composition and distribution are controlled by source areas in Mexico and Baja California, and by the Tamayo Fracture Zone, which acts as a natural boundary between the East Pacific Rise to the south and the complex ridge-transform system of the Gulf of California to the north.

To the east, the source of the sediments is mainland Mexico. The Oligocene-Miocene ignimbrite flows of the Sierra Madre Occidental overlie disconformably large plutonic bodies of Late Cretaceous age. These rocks intrude through Early-Middle Cretaceous volcanic-volcaniclastic material (equivalent to the Alisitos formation), which was strongly deformed during the Middle Cretaceous. As a result of tropical climate and the young morphology of the Sierra Madre Occidental, large amounts of clastic material are supplied to the mouth of the Gulf of California.

To the west, the La Paz Block at the tip of Baja California shows a more evolved morphology and a more arid climate. In this area, Tertiary volcanism (represented by the Comondú Formation) is less developed than in the Sierra Madre Occidental to the east. A marine-to-continental Pliocene sequence lies disconformably on top of Late Cretaceous plutonic rocks intruding late Paleozoic metamorphics.

Between these two land masses, the oceanic crust, which is nowhere older than 3.5 m.y., was subjected to a high sedimentation rate during its formation at the ridge crest. Thus, the magmatic and sedimentary processes are intimately linked in this area.

Seismic profiles in the area (Lewis, 1979) and fine-scale studies on the ridge crest to the south at 21°N (Cyamex Scientific Team, 1981; Rangin and Francheteau, 1981) reveal that flat basement surfaces alternate along the strike of the ridge with rough topography. The high relief consists of pillow basalts, whereas flat basements are formed by sheet flows and massive lavas. These different types of volcanism were interpreted as volcanic cycles occurring on the axis of the East Pacific Rise (Rangin and Francheteau, 1981). A similar setting was described by van Andel and Ballard (1979) at the Galapagos Ridge Crest. Massive flows with smooth topography are thought to be produced rapidly during a flooding episode on the valley floor. In contrast, pillow basalts appear to represent a slower outpouring on the ridge axis. Sites 482, 483, and 485 were drilled on these flat basement surfaces.

Detailed studies at the crest of the East Pacific Rise at 21°N (Cyamex Scientific Team, 1981) reveal that these massive flows were emplaced in a 2- or 3-km wide strip along the ridge axis and that no extrusive activity occurred off-axis. At the mouth of the Gulf (Fig. 1), the sediments overlying the uppermost basaltic unit increase regularly in thickness outward from this active tectonic zone. This supports the idea that the sediments found interlayered with basalts in the basement on Leg 65 were accumulated on the seafloor along the axis of the ridge. Nevertheless the occurrence of sills and dykes cannot be discounted (Schmincke et al., this volume).

[1] Lewis, B. T. R., Robinson, P., et al., *Init. Repts. DSDP*, 65: Washington (U.S. Govt. Printing Office).

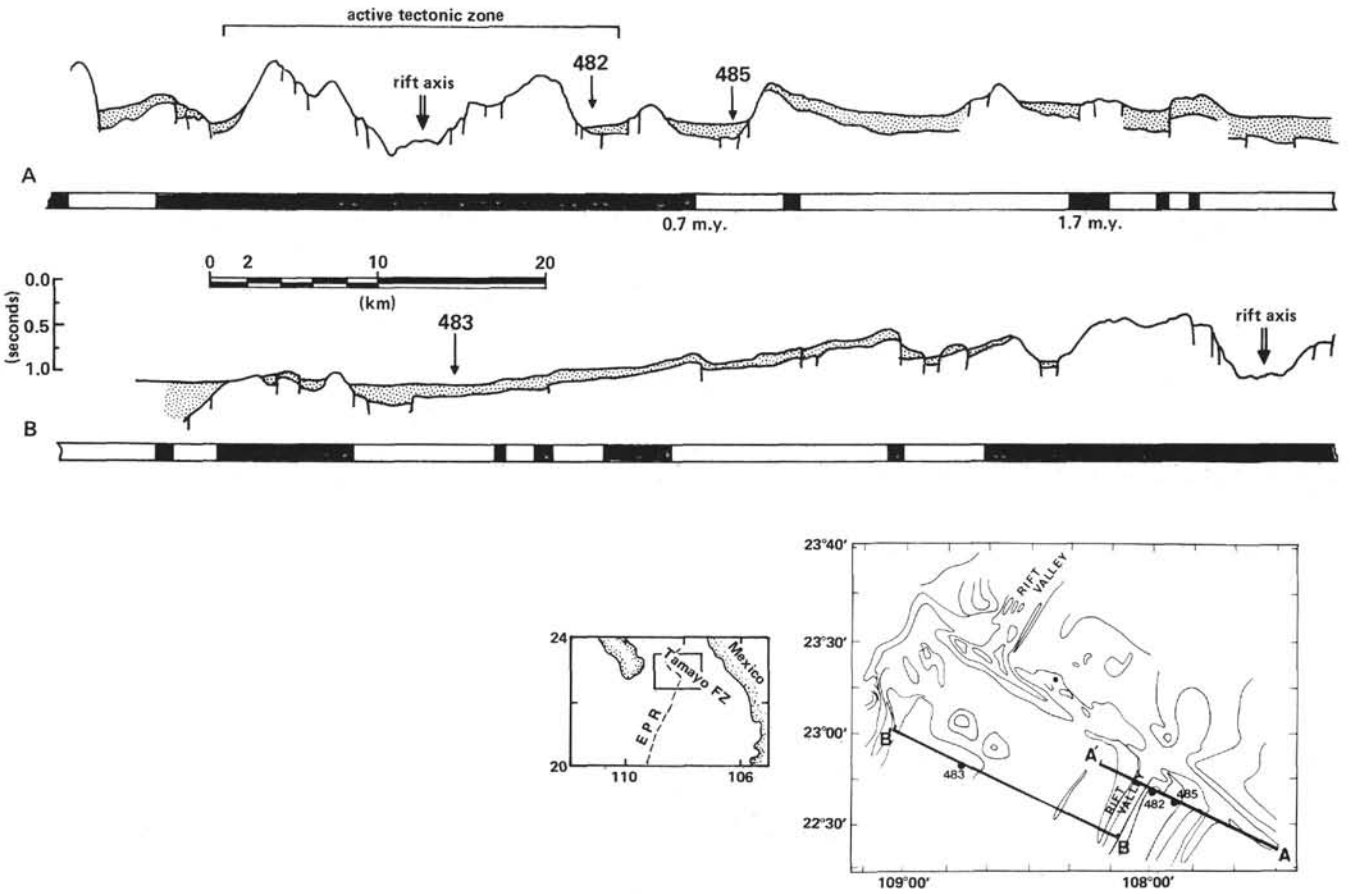

Figure 1. Interpreted seismic profiles over Sites 482, 483, and 485, showing thickness of sediments above basement in seconds of two-way travel time (vertical scale). Horizontal bars show magnetic anomalies. (Inserts show site and profile locations.)

SEDIMENT CHARACTERISTICS

Sediments above Basement

The basement reflector easily identified on Figure 1 corresponds to the uppermost basaltic unit.

Sedimentary cover increases regularly in thickness on both sides of the ridge with distance from the ridge axis (Fig. 1). However sedimentation rate is higher on the continental side (mainland Mexico) than on the Baja California side. This regular increase in sediment thickness implies that no sills or flows are emplaced in the sedimentary cover beyond 12 km of the ridge axis. Sediment lithology is described in detail elsewhere (see site chapters, this volume). Sediments overlying the uppermost basaltic unit are mainly hemipelagic with minor sand and silt interbeds (Fig. 2). Fine-grained turbidites are present, primarily at Site 485, the site closest to mainland Mexico.

The following contact metamorphic processes are recognizable in the sediments near the basement: (1) In Hole 482B dehydration was observed 10 to 14 meters above basement. The same phenomenon occurs in Hole 483, 20 meters above basement, but is only observable 2 to 3 meters above basement in Hole 485A. (2) Hemipelagic sediments, commonly olive gray, change in color near basement (last 2 to 3 m in Hole 483). (3) Dolomite enrichment is observable toward the bottom of the sedimentary section (for example, 2 to 7 m above basement in Hole 482B and 2 m above basement in Hole 482C). Pyrite and zeolite enrichment are also common in sediments in contact with basalt. (4) Carbonate concretions (Hole 482D), hyaloclastites (Hole 483), and small (millimeter-size) patches of volcanic ash are locally present at various depths in the sediments.

Sediments Interbedded with Basalts

In most of the holes drilled, hemipelagic sediments similar to those described were found interlayered with the massive basalts and occasional pillow basalts lying below the uppermost sediment/basalt contact. The thickness of the sedimentary layers was established from logging and drilling records. The sediments were poorly recovered at Sites 482 and 483 (Figs. 3, 4). The thickest sedimentary layers were encountered at Site 485. Because of the high pumping rates in drilling through the basalts, the sediments lying just below the basalt units were not recovered; only the sediments lying directly above the basalts were sampled.

HEMIPELAGIC TERRIGENOUS SEDIMENT

About 50 samples of the sediments overlying the basement, interbedded between the various basement cooling units and in contact with basalts, were analyzed.

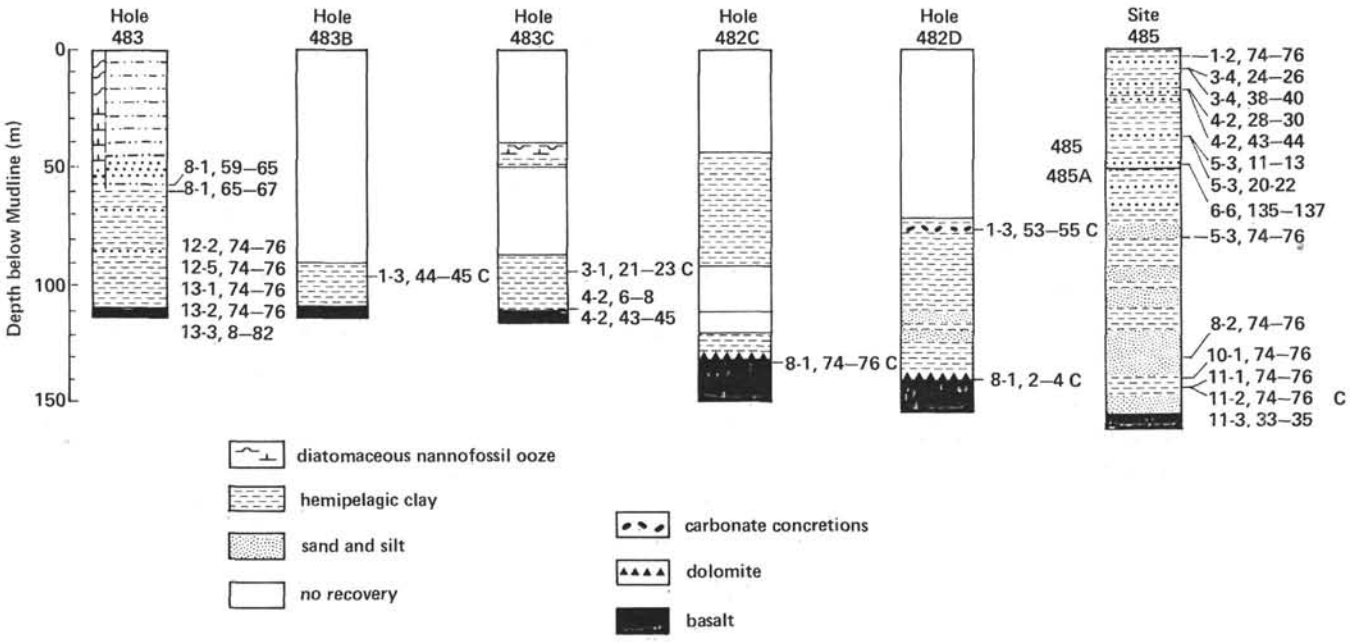

Figure 2. Locations of analyzed samples from sediments above basement. (C, close to sample number, indicates carbonate analysis.)

The objectives were: (1) To determine the nature of the sediments on both sides of the East Pacific Rise and to relate sediment composition to source areas and emplacement processes; and (2) To investigate basalt–sediment interactions as indicated by mineralogical and chemical changes of sediments close to cooling units.

METHODS

We analyzed the bulk sediment and the <2 μm, <0.5 μm, and <0.1 μm clay fractions after they were separated by centrifugation. The analyses were performed by X-ray diffraction and with a Scanning Electron Microscope having an X-ray dispersive attachment (SEM/EDAX).

The clay mineralogy is indicated by the ratio of the areas under the main phyllosilicate peaks, and the d(060) spacing indicates whether the clays are di- or trioctahedral.

The results obtained by SEM/EDAX analysis were only semiquantitative. The relative error is 5% for the major elements ($\geq 10\%$ by weight); 10% for elements between 10% and 5% by weight; and 20% for minor elements ($\leq 5\%$). All results expressed as oxides were normalized to 100%, disregarding hydroxyls and residual water.

Results: Sediments Not in Contact with Cooling Units

1. *Holes 485 and 485A*. From mudline to Core 20 in Holes 485 and 485A, the mineralogy of the sandy fraction shows a constant ratio of quartz to feldspar, and the clay fraction contains dioctahedral smectites, illite, and clinoptilolite (Table 1). From Core 20 to Core 38 in Hole 485A, chlorite is present, but clinoptilolite was not detected. Although the mineralogical change coincides with a transition from turbidite-bearing deposits to predominantly hemipelagic sediments, carbonates are present throughout the section.

The smectites found in the upper part of the section belong to the ≤ 0.1 μm clay fraction. According to the Reynolds and Hower method (1970), these smectites are composed predominantly of expandable layers (70–80%), which SEM/EDAX analyses reveal are similar to Al-beidellite (Table 2).

2. *Hole 483*. Sediments from this hole have the same quartz–feldspar ratio as in Hole 485 and 485A, but carbonates are absent. Incipient clinoptilolite is also noted. The main difference between Sites 483 and 485 is revealed by the composition of the clay fraction. The ratio of dioctahedral smectite to other phyllosilicates (illite–chlorite) is lower on the eastern side of the East Pacific Rise than on the western side. On the other hand, kaolinite, which is present in small amounts at both sites (in association with random mixed-layer minerals and some palygorskite), is more abundant in Hole 483 than Hole 485A.

As at Site 485, the smectites belong to the <0.1 μm clay fraction and consist of Al-beidellite (Table 2). These smectites are not as well "crystallized" as in Hole 485A. Their expandable layer content is not over 50 to 60%.

3. *Discussion*. Clay minerals of detrital origin (mainly illite and chlorite) are more abundant on the eastern side of the East Pacific Rise than on the western side. At the same time, the smectites on the western side have a lower content of expandable layers.

For Site 483, the closest source area is located at the tip of Baja California, which is composed mainly of calc-alkalic intrusive rocks. The detrital source area for Site 485 is in the Sierra Madre Occidental, where ignimbrite flows are widespread. No fundamental chemical differences exist between these two terrains, but volcanic material is more easily hydrolyzed than intrusive rocks, and smectites are the most common secondary minerals in the Sierra Madre Occidental.

Sediments in Contact with Cooling Units

Several sedimentary sequences in contact with basalt or interbedded between basalt cooling units were studied in detail. These sequences can be roughly divided into two types: (1) sedimentary units with mineralogical and

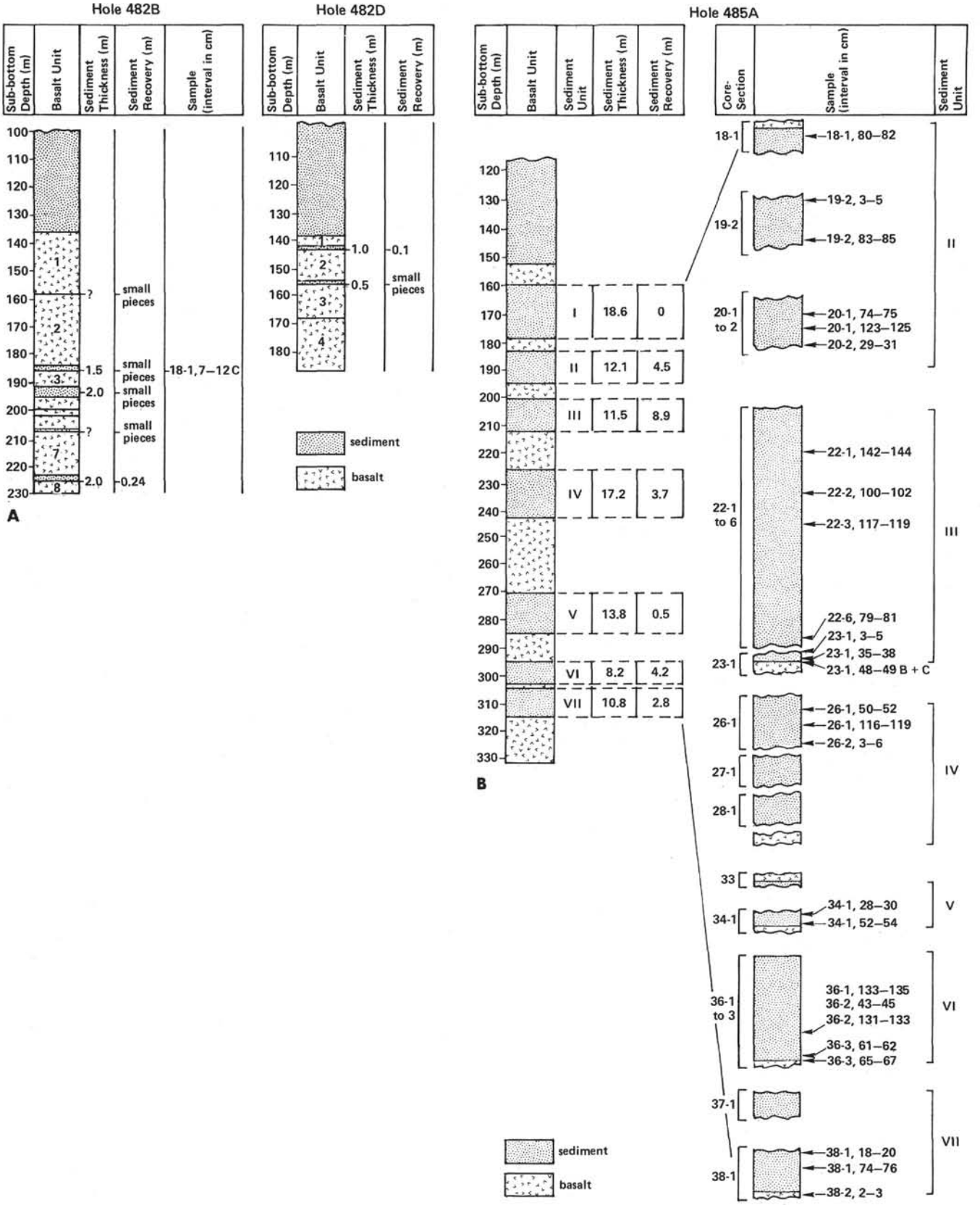

Figure 3. A. Locations of analyzed samples in sediments interbedded with basalts at Site 482. (C indicates carbonate analysis.) B. Locations of analyzed samples in sediments at Site 485. (B and C, close to sample numbers, indicate basalt and carbonate analyses, respectively.)

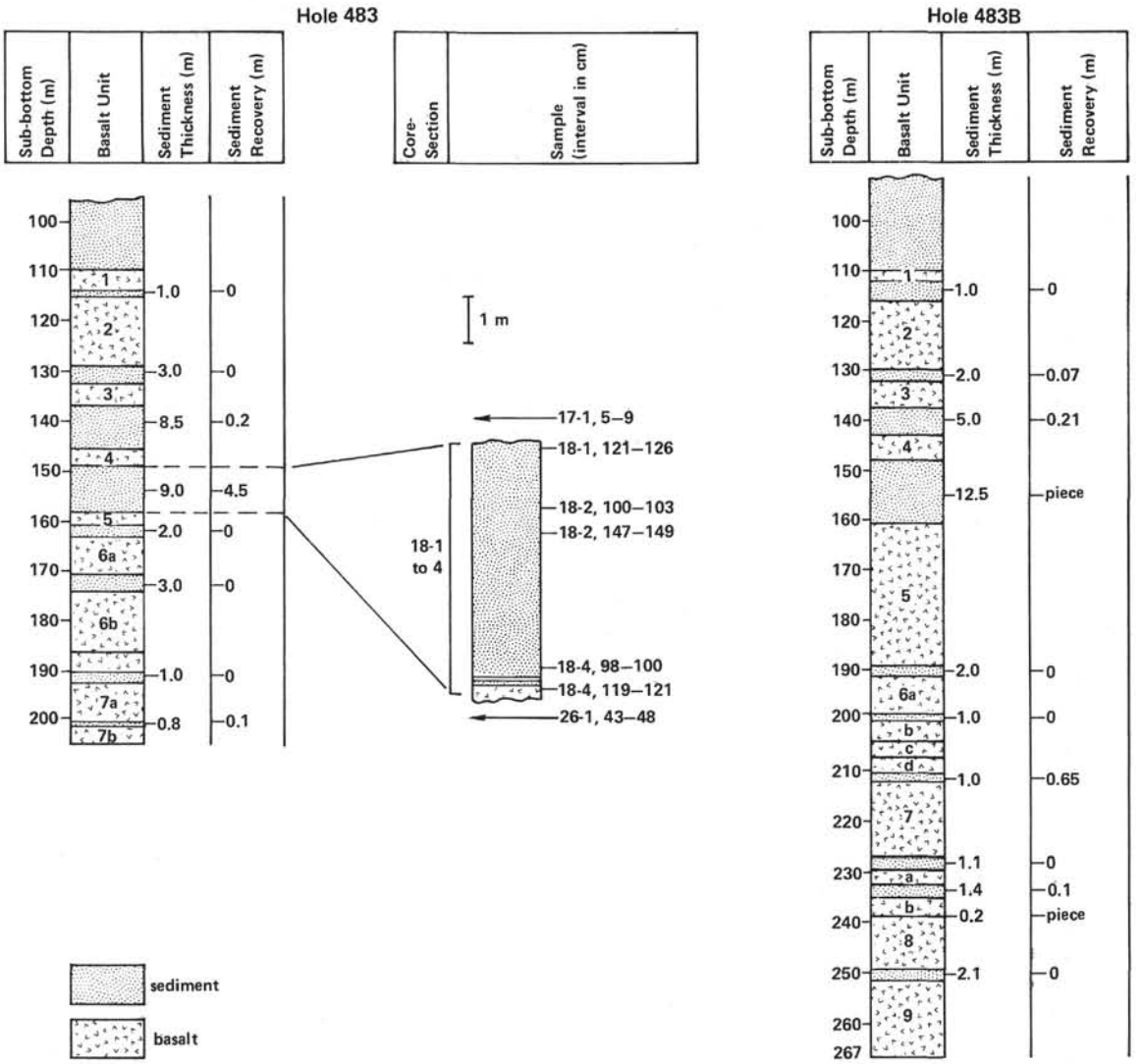

Figure 4. Locations of analyzed samples in sediments interbedded with basalts at Site 483.

Table 1. Mineralogy of the clay fraction in hemipelagic and terrigenous sediments from Sites 483 and 485.

Hole	Sample(s)	Weight %				Smectites		Zeolites	
		Illite	Chlorite	Mixed-Layer Chlorite-Smectite	Smectite	Al-rich Smectite	FeMg-rich Smectite	Clinoptilolite	Analcite
Hole 485	Average of 8 analyses	19	tr	—	81	X	—	X	—
Hole 485A	Cores 5 to 20; 8 analyses	13	tr	—	87	X	—	X	—
	Cores 20 to 38; 7 analyses	8	9	—	83	X	—	—	—
Hole 483	Cores 12 to 26; 11 analyses	24	23	—	53	X	—	tr	—
	23-1, 3–5 cm	7	7	—	86	X	—	—	—
	23-1, 35–38 cm	5	5	41	49	X	—	—	X
Sediments in Contact with Cooling Units	34-1, 28–30 cm	6	6	—	88	X	—	—	—
	34-1, 52–54 cm	6	10	—	84	—	X	—	X
	36-3, 61–62 cm	7	13	—	80	X	—	—	—
Hole 485A	36-3, 65–67 cm	10	10	tr	80	X	X	—	—
	38-1, 18–20 cm	7	7	—	86	X	—	—	—
	38-1, 74–76 cm	10	10	40	40	X	X	—	X
Hole 483	26-1, 43–48 cm	23	9	—	68	—	X	—	—
Hole 483C	4-2, 6–8 cm	18	25	—	57	X	—	—	—
	4-2, 43–48 cm	15	5	—	80	—	X	—	—

Table 2. Structural formulas of clay minerals extracted from sediments based on SEM/EDAX analysis.

Mineral	Sample (interval in cm)	[Si	Al	Fe^{+3}]	[Al	Fe^{+3}	Mg]	Mg	K	Na
1	Hole 485A average of 17 analyses	3.79	0.21		1.44	0.31	0.24	—	0.11	0.37
2	485A-34-1, 52–54	3.21	0.79		0.44	0.83	1.15	0.17	0.06	0.38
3	483-26-1, 43–48	3.15	0.85		0.79	0.82	0.58	0.20	0.41	0.05
4	485A-23-1, 35–38	2.79	1.21		0.43	1.10	0.70	0.57	0.08	—
5	483C-4-2, 43–45	3.29	0.38	0.33	—	0.93	1.58	—	0.01	0.75

Note: 1 = Al-beidellite; 2, 3 = chlorite-smectite, randomly mixed, 80% expandable; 4 = corrensite; 5 = FeMg saponite. Clay fraction ≤ 0.1 μm; Na-saturated.

chemical characteristics similar to those described above; and (2) indurated sediments in direct contact with basalts or separated from them by carbonate coatings or beds.

In Hole 485A, the transition from the first to the second of these types is marked by a constant SiO_2 to Al_2O_3 ratio, a constant K_2O to CaO ratio, and a minor but significant enrichment in MgO, FeO, and Na_2O (Table 3). Similarly, the quartz to feldspar ratio is constant over this interval, and illite and chlorite are always present though the dioctahedral smectites disappear. In addition, the indurated sediments typically contain fine-grained, authigenic Na-zeolites (analcite), and well crystallized Mg–Fe clay minerals, belonging to the ≤ 0.5 μm clay fraction. These clays display the various stages between Mg-smectites and a (mixed-layer) chlorite–smectite. The mixed-layer chlorite–smectite shows all characteristics of a "corrensite," with regular alternation of expandable layers and layers with brucite sheets. From X-ray diffraction studies of the 060 spacing, the Mg-smectite can be considered as a saponite. However, the presence of migrating 001 peaks during heating and treatment with ethylene glycol allows us to interpret this smectite, particularly the ≤ 0.1 μm fraction, as a random mixed-layer chlorite–smectite with a high percentage (80–90%) of expandable layers. Structural formulas deduced from analyses of Na-saturated samples indicate substantial Si–Al substitution in the tetrahedral sheet, beyond the generally accepted limits for saponites, as well as the presence of Mg in the brucite sheet. At Site 485, the disappearance of detrital dioctahedral smectite coincides with the genesis of Mg–Fe expandable mixed-layer phyllosilicates. In this context, we observe a rather constant ratio of the smectites through the transition to indurated sediments, at least before the appearance of corrensite.

The indurated sediments at Site 483 have two distinct mineralogical assemblages. As in Hole 485A, the indurated sediments interlayered with the basalts (e.g., Sample 483-26-1, 43–48 cm) contain random mixed-layer chlorite–smectites with 80% expandable layers. When compared with unaltered sediments, the mineralogical assemblage indicates a relative decrease of the chlorite content, but no chemical variation was observed. In other samples, however (e.g., Sample 483C-4-2, 43–45 cm), saponite is well developed. In this case, the indurated sediment can be distinguished from nonindurated sediments on the basis of the spectrum of major elements (Table 3). As in Hole 485A, dioctahedral Al-smectite is "replaced" by Fe–Mg expandable phyllosilicate minerals. The decrease in chlorite content again implies a relative increase in the smectite content. Analcite, however, was not detected at this site.

Discussion

The sediments at Sites 483 and 485 lie directly on cooling units without any intervening occurrence of thick hyaloclastite layers. This observation is confirmed by chemical and mineralogical analysis of sediments in direct contact with basalts. The only exception was Sample 483C-4-2, 43–45, the chemical content of which could indicate the presence of altered glassy fragments within the sediment.

In the sediments in contact with basalts, secondary formation of Fe–Mg clay minerals (saponite and random mixed-layer chlorite–smectites) is observed. This authigenesis is accompanied by the disappearance of dioctahedral Al-smectite, but mica and feldspar are not modified. Al-smectite can be considered as a source for the Al and Si necessary for Fe–Mg clay mineral, and perhaps analcite, formation.

Al and Si can also be provided by chlorite, which in some cases (Site 483) is disappearing along with the Al-smectite. They might also be introduced by hydrothermal systems related to the cooling-unit emplacement pro-

Table 3. Bulk SEM/EDAX analyses of terrigenous hemipelagic sediments from Sites 483 and 485.

	Hole 485A							Hole 483			Hole 483C	
	Sample (interval in cm)											
Major Oxide	11-1, 74–76	34-1, 28–30	34-1, 52–54	23-1, 3–5	23-1, 35–38	38-1, 18–20	38-1, 74–76	12-2, 74–76	18-1, 43–48	18-4, 98–100	4-2, 6–8	4-2, 43–45
Na_2O	0.6	1.6	2.4	1.2	2.6	1.0	3.0	—	1.1	0.7	0.1	0.1
MgO	1.2	2.1	3.9	1.5	1.8	1.7	2.3	2.9	2.2	2.9	2.0	7.0
Al_2O_3	17.8	17.9	16.4	17.9	15.3	17.9	18.5	19.2	16.6	18.1	18.2	12.8
SiO_2	62.9	59.5	58.5	60.8	59.9	60.0	62.7	61.8	65.1	60.8	62.6	59.6
SO_3	1.0	2.0	0.4	1.5	1.6	1.6	0.3	1.5	—	0.8	1.8	—
Cl	—	1.7	0.5	0.8	0.7	—	0.3	—	—	—	—	—
K_2O	4.0	4.5	4.0	3.9	3.9	4.9	5.1	3.6	5.7	5.8	5.1	2.6
CaO	4.8	3.6	5.6	5.2	5.5	5.6	1.0	0.7	1.3	1.9	0.9	1.3
TiO_2	0.7	0.9	0.6	0.8	1.2	0.8	0.8	0.4	0.8	0.7	0.5	0.7
FeO	7.0	6.2	7.7	6.4	7.6	6.5	6.0	9.9	7.2	8.3	8.8	15.9

cess (the slight Fe–Mg enrichment detected in sediments in contact with the basalts is in agreement with such a hypothesis). Finally, the Al and Si might be derived from glassy fragments irregularly distributed in the sediments in contact with the basalts, though not presently observable because already transformed into secondary minerals.

In any case, all the observed changes in sediments are located near the contacts with the basalts. Data obtained by Kristmannsdóttir (1976) and Kristmannsdóttir and Tómasson (1978) in the Reykjanes geothermal area in Iceland indicate that saponite is formed at temperatures below 200°C and that the mixed-layer chlorite–smectites form between 200° and 270°C. Above these temperatures, chlorite forms, but this mineral was not found in the Leg 65 sites. On the other hand, analcite is stable between 70 and 300°C.

ALTERATION PRODUCTS OF VOLCANIC GLASSES (basalts in contact with sediments and hyaloclastites)

In addition to the sediments discussed above, we have examined several thin cooling-unit margins coated with sediments from Hole 485A (Samples 485A-23-1, 48–49 cm; 485A-36-3, 65–67 cm, and 485A-38-2, 2–3 cm; Fig. 3). The sediments in contact with the basalts show all the modifications described previously. Furthermore, the alteration products of a hyaloclastite sample (Sample 483-8-1, 59–65 cm; Plate 3), found interbedded with unaltered sediment, were also studied in detail.

Cooling Unit Margins in Contact with Sediment

The cooling-unit margins examined from Hole 485A may be divided into two distinct textural zones (Plates 1, 2). These include a thin (<0.5-cm thick) aphyric glassy zone which has been largely altered to green, orange, or beige palagonite, but which also contains calcite patches and numerous varioles and spherulites in the less altered portions of this zone, and a microlitic zone where plagioclase microlites (An 70–90) are distributed through a more-or-less altered interstitial glass. These microlites are associated with occasional phenocrysts of plagioclase (An 90–100) and augite. The plagioclases and Fe–Mg minerals are unaltered.

Although the microlitic and glassy zones are roughly concentric, the glassy zone extends through the microlitic zone along fissures filled with calcite and sulfides.

In addition to the features discussed, a 1-mm thick calcite layer and a fine-grained, greenish calcareous sandstone are present at the basalt/sediment contact on top of Cooling Unit 4 in Hole 485A (Sample 485A-23-1, 48–49 cm; Plate 4). The sandstone is composed of pyroxenes and partially to totally altered plagioclase grains (An 70–90) distributed within a calcite cement. This material is well bedded, and could represent an altered hyaloclastite.

Chemical Effects of Alteration

Various interstitial glass areas from microlitic and glassy zones were analyzed by SEM/EDAX. These areas show both homogeneous and heterogeneous alteration textures depending on the presence or absence of secondary minerals. "Fresh and altered glass" will refer to the apparently homogeneous mesostasis, without or with K_2O, respectively (Table 4).

1) *Altered glasses.* Assuming that Al is immobile during alteration, the microlitic zone shows a loss of CaO related to K_2O enrichment and a slight Na_2O, MgO, and Fe enrichment which may not be significant considering the analytical method used here. In contrast, the glassy zone displayed a strong K_2O, MgO, and Fe_2O enrichment, a total loss of Na_2O, and a nearly total loss of CaO.

2) *Glasses with secondary minerals.* The microlitic zone displays intensive glass alteration which produces a heterogeneous texture. Concentric and bedded aggregates of secondary minerals which concentrate Na_2O and CaO or FeO–MgO and TiO_2 are observed, and geodes filled with well-crystallized minerals representative of the bulk composition of the aggregates are distributed. Zeolites (chabazite) and Fe–Mg minerals are also present.

Mineralogy of Secondary Alteration Products

The presence of chabazite, trioctahedral smectites with varying percentages of expandable layers, and minor chlorites was confirmed by X-ray diffraction. SEM/EDAX analyses of the aggregate minerals indicate the presence of Ca–Na rich chabazite and minor smectites of the Al-beidellite type (Tables 5, 6). However, these smectites frequently show chlorite–smectite interlayering. In these cases, their structural formulas indicate that they are identical to the mixed-layer trioctahedral chlorite–smectite previously described in the altered sediments in contact with basalts; nevertheless, they are K rich. Some of the K is also present in celadonitic(?) illite–mica interlayering detected by X-ray but not observed with the SEM/EDAX.

Hyaloclastites in Sediments

For the most part the vitric fragments found in the Leg 65 sediments are very fresh (sideromelane); they have numerous vesicles and show a very thin chilled margin (Plate 3). Other fragments appear strongly hydrolyzed, leading to nearly total glass dissolution, in which case the chilled margin is only preserved around cavities. Other fragments show cavities filled with clay mineral pellets.

Various sideromelane alteration stages from palagonite to clay pellets were studied. These fragments show increasing palagonitization marked by a loss of Na_2O–CaO and an enrichment in K from their cores to their rims. At the same time, the FeO and MgO contents respectively increase and decrease. Pellets representing the most advanced alteration stages consist of Fe-beidellite.

Discussion

From the preceding discussion, it is clear that the alteration of basaltic glass can be distinguished from hyaloclastite alteration on the basis of their respective changes in chemistry and the composition of their alteration products. The fractionation and reorganization

Table 4. Composition of basaltic glass and hyaloclastites based on microprobe analysis.

	Basalt (Sample 485A-38-2, 2-3 cm)				Basalt (Sample 485A-36-3, 65-67 cm)					Hyaloclastite (Sample 483-8-1, 59-65 cm)		
	Microlitic Texture			Glassy Rim	Microlitic Texture				Glassy Rim	Core		Rim
Major Oxide	Fresh Glass	Altered Glass	Zeolite-rich Glass	Palagonite	Fresh Glass	Altered Glass	Palagonite	Zeolite-rich Glass	Palagonite	Fresh Glass	Altered Glass	Palagonite
Na_2O	3.4	3.7	5.7	—	4.2	6.1	0.3	6.9	—	1.9	1.2	—
MgO	3.7	5.0	0.5	11.4	2.3	2.4	6.6	—	10.0	7.5	5.8	16.5
Al_2O_3	23.8	23.8	25.7	17.7	25.7	20.6	22.6	22.0	20.8	15.8	15.4	15.2
SiO_2	53.5	52.5	56.9	43.2	51.5	59.3	51.3	64.0	66.3	50.7	58.0	56.0
K_2O	—	0.9	0.2	6.6	—	0.5	0.3	0.2	3.5	—	2.0	1.4
CaO	6.3	5.1	7.6	0.8	7.8	2.0	1.4	5.5	0.7	12.5	2.7	1.5
TiO_2	2.7	2.3	2.0	2	2.8	2.0	5.0	0.2	3.6	1.2	0.4	1.1
FeO	6.6	6.7	1.4	18.3	5.7	7.1	12.5	1.2	15.1	10.4	14.5	8.3

Table 5. Average composition of zeolite and clay minerals in basalt and hyaloclastite based on SEM/EDAX analysis.

Major Oxide	Mineral 1	2	3	4	5	6	7
SiO_2	55.7	64.2	61.3	51.8	48.2	40.5	48.0
Al_2O_3	27.5	24.8	19.1	19.9	17.8	16.7	17.6
FeO	0.8	3.2	8.5	9.3	10.8	20.5	14.5
MgO	—	5.1	2.9	9.4	14.8	12.9	18.9
CaO	11.0	0.8	0.7	4.2	1.8	1.2	0.4
Na_2O	5.1	0.9	4.00	0.3	—	0.2	0.5
K_2O	—	1.0	2.8	2.5	4.0	5.6	0.10
TiO_2	—	—	0.7	2.6	2.6	2.4	—

Note: 1 = chabazite; 2 = Al-beidellite in basalt; 3 = Fe-rich beidellite (alteration products of hyaloclastite); 4–7 = mixed-layer chlorite-smectite.

Table 6. Structural formulas of clays deduced from analyses in Table 5.

Mineral	Element [Si	Al]	[Al	Fe^{+3}	Mg]	Mg	Ca	Na	K
2	3.79	0.21	1.52	0.16	0.44	—	0.05	0.11	0.07
3	3.79	0.21	0.61	1.44	0.26	—	0.05	0.47	0.22
4	3.35	0.65	0.85	0.50	0.89	—	0.29	0.02	0.20
5	3.15	0.85	0.52	0.60	1.31	0.12	0.13	—	0.34
6	2.77	1.23	0.12	1.18	1.05	0.26	0.08	0.03	0.49
7	3.02	0.98	0.34	0.77	1.31	0.43	0.05	0.04	0.01

of the elements liberated during glass hydrolysis and extracted from the alteration fluids can be observed within the basalts at the sediment/basalt contact. These elements have gone mainly into Na–Ca rich zeolites, mixed-layer chlorite-smectites, and to a lesser extent, into dioctahedral smectites.

Although hyaloclastites show roughly the same chemical composition as the glassy material previously described, the hyaloclastites studied here have undergone a different evolution involving the loss of Na, Ca, and Mg and the formation of Fe-beidellite. It should be pointed out, however, that these samples have only undergone low temperature alteration.

Earlier studies of submarine basalt alteration (e.g., Ijima and Harada, 1969; Bass, 1976) have concluded that di- and trioctahedral smectites are typical of low temperature alteration, or halmyrolysis (Melson and Thompson, 1973; Andrews et al., 1977; Seyfried et al., 1976; Robinson et al., 1977; Juteau et al., 1980) and that mixed-layer chlorite–smectites, associated with zeolites such as analcite, are index minerals for hydrothermal alteration (Humphris and Thompson, 1978). The samples studied here show trioctahedral smectites replaced by mixed-layer minerals.

This suggests that low temperature alteration has been superimposed over an earlier stage of hydrothermal alteration. This interpretation is supported by chemical changes which show a loss of Na and Ca and an enrichment in K, Mg, and Fe, chiefly in the glassy rims. These various enrichments and losses characterize low and high temperature alteration processes (Scott and Hajash, 1976; Seyfried and Bischoff, 1979). As noted previously, it is possible that some of the Na and perhaps the Fe-Mg could have migrated from the basalt via alteration fluids into the overlying sediments, leading to formation of analcite and trioctahedral minerals.

STABLE ISOTOPE CONTENT OF CARBONATES AND ORGANIC MATTER

The stable isotope content (^{18}O and ^{13}C) of selected carbonate samples was measured in order to evaluate the environmental conditions during crystallization or recrystallization (Table 7). The samples include calcareous mud (Sample 485A-11-2, 74–76 cm), calcareous concretions (Sample 483B-1-3, 44–45 cm, Sample 483C-

Table 7. Stable isotope content of carbonate from Sites 482, 483, and 485.

Mineral	No.	Sample (interval in cm)	^{13}C vs. PDB	^{18}O vs. PDB	^{18}O vs. SMOW
Calcite	1	485A-11-2, 74-76	+0.92	+0.41	+31.20
	2	483B-1-3, 44-45	−14.86	+1.03	+31.92
	3	483C-3-1, 21-23	−15.56	−0.88	+29.95
	4	485A-23-1, 48-49	−35.96	−5.34	+25.36
	5a	485A-38-2, 2-3	−11.80	−7.56	+23.07
	5b		−13.36	−9.10	+21.48
			−12.65	−7.20	+23.44
Dolomite	6	482B-18-1, 7-12	−9.75	−8.86	+21.73
	7	482D-1-3, 53-55	+0.33	+5.64	+36.67
	8	482D-8-1, 2-4	+0.36	+6.22	+37.27
	9	482C-8-1, 74-76	−12.10	+0.60	+31.48

Note: 1 = hemipelagic sediment; 2, 3 = concretions; 4 = calcareous sandstone in contact with basalt; 5a = calcite patches in glassy basalt; 5b = calcite veins in cooling unit margin; 6 = geode in fresh basalt; 7 = dolostone concretions in sediment; 8, 9 = dolostone beds in contact with basalt.

3-1, 21–23), and dolomitic nodules (Sample 482D-1-3, 53–55), located several tens of meters from any basaltic units. Indurated carbonates in contact with the basalts or in veins in the margins of the cooling units were also investigated. These were either calcareous (Sample 485A-23-1, 49–49 cm, Sample 485A-38-2, 2–3 cm), or dolomitic (Sample 482D-8-1, 2–4 cm, Sample 482C-8-1, 74–76 cm).

The ^{13}C content of the organic matter in samples taken at approximately the same levels was also measured in order to investigate the evolution of the initial organic matter under the influence of heating by basaltic intrusions (Table 7).

Carbonates

General Environment: Total Dissolved Organic Carbon and the Effect of Temperature

The samples examined exhibit large variations in both ^{13}C and ^{18}O. The calcareous mud (Sample 485A-11-2, 74–76) has an isotope composition which is quite representative of common marine carbonates in terms of both ^{18}O and ^{13}C content. The calcareous concretions are largely depleted in ^{13}C as compared to normal marine calcite, whereas their ^{18}O contents are compatible with local sea bottom conditions. Oxygen 18 values suggest that crystallization occurred between 13 to 19°C in normal seawater ($\delta^{18}O \simeq 0$). The depletion in ^{13}C results from the major influence of CO_2 of biogenic origin within the environment. At 15 to 20°C, the fractionation factor between CO_2 and calcite is approximately 10‰ (Friedman and O'Neil, 1977). Calcite crystallization in equilibrium with an open system would thus have required an environmental CO_2 with a ^{13}C content of about −25‰. Because of the local conditions of crystallization (pore solutions in poor contact with dissolved gases and buffering conditions of pH), it is likely, however, that crystallization occurred in a closed system. In that case the ^{13}C content of the carbonate would be that of aqueous CO_2. Thus, the $\delta^{13}C$ values of the carbonate concretions could indicate mixing between biogenic carbon and marine dissolved carbon.

The indurated calcites studied are depleted in both ^{13}C and ^{18}O. The depletion in ^{18}O can theoretically reflect either an input of continental waters or a temperature effect (the influence of fluctuations in the heavy isotope content of ocean water may be ruled out since an effect would not have accounted for more than 2‰ of the variations, whereas values as low as −9‰ are observed). The input of continental water through the sea bottom is possible when allowed by the hydraulic head of coastal aquifers. This process was held to account for the low ^{18}O content of Messinian diagenetic carbonates in the Mediterranean (Pierre and Fontes, 1979). However, because of the location of the indurated calcites studied on the basaltic intrusions, their low ^{18}O content is attributed to temperature.

Temperature Estimation from Isotope Data

In seawater ($\delta^{18}O \simeq 0$ vs. SMOW), the temperatures calculated from the fractionation values listed by Friedman and O'Neil (1977) range between 50 and 65°C. However, the ^{18}O content may have been modified by two antagonistic processes during and after the intrusion of the cooling units. The first process is an isotope exchange between rock, minerals, and water during the intrusion. The ^{18}O content of the unaltered intrusive basalt is probably close to −6‰ (Muehlenbachs, 1971). At intrusion temperatures (≥400°C) the resulting fractionation factor between rock mineral components and water is about 2‰ (Friedman and O'Neil, 1977). Thus the initial seawater ($\delta^{18}O \simeq 0$) could be enriched by approximately 4‰ during a complete isotope exchange process. Even in that case the corresponding calculated temperature would not exceed 100°C for the most ^{18}O-depleted sample (Sample 485A-38-2, 2–3 cm).

The second process is the diagenetic crystallization of magnesian clays and zeolites. This process gives rise to an ^{18}O depletion which can reach 10‰ in the pore fluids (Lawrence, 1974; Lawrence et al., 1975; Gieskes et al., 1978; Randall et al., 1979). In the case of such an ^{18}O-poor fluid, the crystallization temperature would not have exceeded 15°C for the most ^{18}O depleted calcites. Owing to the lack of data on the interstitial water chemistry, however, it is not possible to discuss in further detail any possible change in the heavy isotope content of the pore fluids stemming from exchange or diagenesis (or even continental water input).

Another argument for relatively low temperature crystallization of carbonates is provided by the oxygen isotope composition of the dolomites in contact with the basalts. The high ^{18}O content of Samples 483D-8-1, 2–4 cm and 482D-1-3, 53–55 from the sediments above basalt may be explained by isotopic fractionation between calcite and dolomite (Fritz and Smith, 1970). Both samples show a high ^{18}O content which can account for this fractionation effect, even though it has not been calibrated for sedimentary temperatures. Numerous field data and extrapolation of high temperature experimental data (Northrop and Clayton, 1966) suggest, for example, that the enrichment in ^{18}O in dolomite, with respect to coexisting calcite crystallized under the same environmental conditions, lies within the range 3 to 6‰. Corrected for such an effect, the $\delta^{18}O$ values of the two dolomites enriched in ^{18}O range again within normal values for sea bottom carbonates. This is in agreement with the fact that dolomite in contact with the basalt (Sample 482D-8-1, 2–4 cm) shows approximately the same ^{18}O content as dolomitic nodules (Sample 482D-1-3, 53–55 cm) included in sediments.

In contrast, the indurated dolomitic layer in contact with the basalt at Sample 482C-8-1, 74–76 shows a depletion in ^{18}O with respect to the dolomite discussed above. This depletion is attributed to a thermal effect which, in any case, will be even lower than that reflected by indurated calcite. Thus, dolomite either does not reflect the thermal effect or shows it rather attenuated. This may result from the lower rate of crystallization of dolomite as compared to calcite, in which case dolomite crystal completion would occur when the intrusion is significantly cooled, using Mg^{2+} ions released by basalt alteration.

Origin of CO_2

Since low ^{13}C contents of carbonates are observed in the vicinity of cooling units, it may be that the production of ^{13}C depleted CO_2 is related to the heat source. The depletion reaches $-36‰$ in Sample 485A-23-1, 48–49 cm which is located upon Cooling Unit 4, more than 210 meters within the hole and is the deepest sample studied. This value cannot be attributed to CO_2 resulting from simple oxidation of marine (or continental) organic matter. It corresponds to the range observed for the light hydrocarbons C_1 to C_4 (see Deines, 1980). Thus, light hydrocarbons formed under the influence of the heat flux in the area are oxidized to give ^{13}C depleted CO_2. Since the porous sediments contain dissolved oxygen from seawater in the most superficial and coolest parts of the system, this oxidation occurs within the sediments near the mudline. In that zone, as previously stated, mixing also occurs with dissolved carbon of marine origin. Samples 485A-11-2, 74–76, 482D-1-3, 53–55, and 482D-8-1, 2–4 have a ^{13}C content reflecting the pure marine origin of the total dissolved carbon.

Organic Matter

The $\delta^{13}C$ values for the organic material from Hole 485A range between -21.05 and -23.35 vs. PDB, with the lowest values observed in contact with the basalts (Sample 485A-11-3, 33–35 cm and Sample 485A-26-1, 50–52 cm) (Table 8). It should be noted, however, that this depletion is limited to about 2‰, as compared to other samples which exhibit a ^{13}C content close to $-21‰$. No explanation can be proposed for this slight depletion in ^{13}C in organic matter in contact with basalt where the separation of a light hydrocarbon fraction was invoked to explain the very low ^{13}C content of carbonates. The values fall, however, within the range of organic matter from normal marine sediments (Deines, 1980). This is in agreement with the weakness of the thermal effect admitted on the basis of the carbonate study.

SUMMARY AND CONCLUSIONS

The East Pacific Rise can be thought of as a permanent barrier between Baja California and mainland Mexico during Quaternary time.

The sediments in contact with basaltic cooling units have been altered. The processes of contact metamorphism which have occurred are marked by decreasing sediment porosity, *in situ* genesis of Na-zeolite, and detrital dioctahedral smectite recrystallization into saponite and mixed-layer chlorite–smectites. These mixed-layer minerals are formed between 200 and 270°C in present-day hydrothermal systems on land. A comparable clay mineral and Ca–Na zeolite paragenesis was observed in selected cooling unit margins, testifying to an early stage of thermal alteration. On the other hand, hyaloclastites distributed through unaltered sediments some distance from the basalts show low temperature secondary products.

Table 8. Stable isotope content of organic matter from Site 485.[a]

Sample	$\delta^{13}C$ vs. PDB ‰
485A-11-1, 74–76	21.39
485A-11-2, 74–76	21.58
485A-11-3, 33–35	23.16
485A-26-1, 50–52	23.35
485A-26-1, 116–119	22.37
485A-26-2, 3–6	21.30
485A-38-1, 18–20	21.85
485A-38-1, 74–76	21.05

[a] After Rangin et al.

The carbonates in the sections drilled were crystallized in a closed or semiclosed system under the influence of CO_2 of organic origin (i.e., resulting from oxidation of light hydrocarbons) at temperatures much below 100°C. Large variations in the heavy-isotope contents of the carbonates are probably related to sharp temperature gradients within the sediments and possibly to large variations in the heavy isotope contents of pore fluids caused by exchange between silicates and water, and/or the formation of secondary minerals. The organic matter does not show any large deviation from normal marine values, which also suggests evolution at low temperatures.

Discrepancies in the "paleotemperatures" obtained by carbonate isotope studies and those obtained from Al-silicate crystallization temperatures could be explained by contact metamorphism, followed in time by low temperature alteration.

Downhole temperature measurements made during Leg 65 at Site 482, however, indicate a 64°C/100 m temperature gradient in the sediments above basement (Lewis, this volume), and a temperature of $150° \pm 5°C$ was measured at the bottom of Hole 482C. This present temperature gradient cannot explain the metamorphic alteration of the sediments in contact with the basalt, because unaltered sediments were observed between the various cooling units. Furthermore, this temperature gradient cannot be explained by a recent emplacement of the uppermost cooling units as sills, since isotope analysis of dolomite and calcite in contact with these cooling units indicate low temperature conditions.

Einsele et al. (1980) have proposed a sill emplacement process in porous sediments to explain alteration phenomena observed in the Gulf of California (Guaymas Basin) on Leg 64. The hydrothermal activity described there has led to a higher grade of alteration of the sediments than observed at the mouth of the Gulf. Consequently we think that the model of Einsele et al. (1980) is not applicable to the East Pacific Rise. We suggest another mode of emplacement for the cooling units in the Leg 65 area: Geophysical surveys in the vicinity of the Leg 65 sites and additional seafloor data for the East Pacific Rise indicate that the majority of the basalts are flows. We suggest that these flows were emplaced at the ridge axis on top of very porous sediments and have partially penetrated them. At Site 485, the sedimentation rate is relatively high (280 to 625 m/m.y.; Site 485 report, this volume) and turbidites are common; this suggests that flows emplaced at the ridge axis were very rap-

idly covered by sediments before the basalts were completely cooled.

ACKNOWLEDGMENTS

This study was made possible with the financial support of the ATP 4232 CNRS. We thank M. Steinberg and our colleagues on Leg 65 for stimulating discussions and M. Kastner and M. Treuil for critical review of the manuscript. The authors are also grateful to the DSDP for making samples available for this study.

REFERENCES

Andrews, A. J., Barnett, R. L., MacClement, B. A. E., et al., 1977. Zeolite facies metamorphism geochemistry and some aspects of trace element distribution in altered basalts of DSDP, Leg 37. *In* Aumento, F., Melson, W. G., et al., *Init. Repts. DSDP*, 37: Washington (U.S. Govt. Printing Office), 795–810.

Bass, M. N., 1976. Secondary minerals in oceanic basalt, with special reference to Leg 34, DSDP. *In* Yeats, R. S., Hart, S. R., et al., *Init. Repts. DSDP*, 34: Washington (U.S. Govt. Printing Office), 392–432.

Cyamex Scientific Team, 1981. First manned submersible dives on the East Pacific Rise at Lat. 21°N (Project RITA): General results. *Mar. Geophys. Res.*, 4:365–379.

Cyamex Scientific Team, and Pastouret, L., 1981. Submersible structural study of Tamayo Transform Fault. EPR 23°N (Project RITA). *Mar. Geophys. Res.*, 4:381–401.

Deines, P., 1980. The isotopic composition of reduced organic carbon. *In* Fritz, P., and Frontes, J. C. (Ed.), *Handbook of Environmental Isotope Geochemistry* (Vol. 1), Terrestrial Environment: Amsterdam (Elsevier Pub. Co.), 329–406.

Einsele, G., Gieskes, J. M., Curray, J., et al., 1980. Intrusion of basaltic sills into highly porous sediments and resulting hydrothermal activity. *Nature*, 283:441–445.

Friedman, I., and O'Neil, J. R., 1977. Compilation of stable isotope fractionation factors of geochemical interest. Data of geochemistry. *Geol. Surv. Prof. Pap.*, 440 KK.

Fritz, P., and Smith, D. G. W., 1970. The isotopic composition of secondary dolomites. *Geochim. Cosmochim. Acta*, 34:1161–1173.

Gieskes, J. M., Lawrence, J. R., and Galleisky, G., 1978. Interstitial water studies. *In* Talwani, M., Udintsev, G., et al., *Init. Repts. DSDP*, Suppl. to Vols. 38, 39, 40, and 41: Washington (U.S. Govt. Printing Office), 121–134.

Humphris, S. E., and Thompson, G., 1978. Hydrothermal alteration of oceanic basalts by seawater. *Geochim. Cosmochim. Acta*, 42: 107–125.

Iijima, A., and Harada, K., 1969. Authigenic zeolites in zeolitic palagonite tuffs on Oahu, Hawaii. *Amer. Mineral.*, 54:182–197.

Juteau, Th., Noack, Y., Whitechurch, H., et al., 1980. Mineralogy and geochemistry of alteration products in Holes 417A and 417D basement samples (Deep Sea Drilling Project Leg 51). *In* Donnelly, T., Francheteau, J., Bryan, W., Robinson, P., Flower, M., Salisbury, M., et al., *Init. Repts. DSDP*, 51, 52, 53, Pt. 2: Washington (U.S. Govt. Printing Office), 1273–1299.

Kristmannsdóttir, H., 1976. Types of clay minerals in hydrothermally altered basaltic rocks, Reykjanes, Iceland. *Jökull*, 26:30–39.

Kristmannsdóttir, H., and Tómasson, J., 1978. Zeolite zones in geothermal areas in Iceland. *In* Sand, L. B., and Mumpton, F. (Eds.) *Natural Zeolites, Occurrences, Properties, Use:* Oxford (Pergamon Press), pp. 199–220.

Larson, R. L., 1971. Near bottom geophysical studies of the East Pacific Rise crest. *Geol. Soc. Am. Bull.*, 82:823–842.

Lawrence, J. R., 1974. Stable oxygen and carbon isotope variations in the pore waters carbonates and silicates, Sites 225 and 228, Red Sea. *In* Tucholke, B. E., Vogt, P. R., et al., *Init. Repts. DSDP*, 43: Washington (U.S. Govt. Printing Office), 669–675.

Lawrence, J. R., Gieskes, J. M., and Broecker, W. S., 1975. Oxygen isotope and cation composition of DSDP pore water and alteration of layer II basalts. *Earth Planet. Sci. Lett.*, 27:1.

Lewis, B. T. R., 1979. Periodicities in volcanism and longitudinal magma flow on the East Pacific Rise at 23°N. *Geophys. Res. Lett.*, 6(10):753–756.

Melson, W. G., and Thompson, G., 1973. Glassy abyssal basalts, Atlantic Sea Floor near St. Paul's rocks: Petrography and composition of secondary clay minerals. *Geol. Soc. Am. Bull.*, 84: 703–716.

Muehlenbachs, K., 1971. Oxygen isotope studies of rocks from mid-ocean ridges [Ph.D. dissert.]. University of Chicago, Chicago.

Normark, W. R., 1976. Delineation of the main extrusion zone of the East Pacific Rise at lat. 21°N. *Geology*, 4:681–685.

Northrop, D. A., and Clayton, R. N., 1966. Oxygen isotope fractionation in systems containing dolomite. *J. Geol.*, 74(2):174–196.

Pierre, C., and Fontes, J. C., 1979. Oxygène 18, carbone 13, deutérium et soufre 34: Marqueurs geochimiques de la diagénèse et du paléomilieu évaporitiques du Messinien de la Méditerranée. *Bull. Mus. Nat. Hist. Nat., Paris*, 4e sér. 1, section c, (1):3–18.

Randall, S. M., Lawrence, J. R., and Gieskes, J. M., 1979. Interstitial water studies, Sites 386 and 387. *In* Tucholke, B. E., Vogt, P. R., et al., *Init. Repts. DSDP*, 43: Washington (U.S. Govt. Printing Office), 669–674.

Rangin, C., and Francheteau, J., 1981. Fine scale morphological and structural analysis of the East Pacific Rise, 21°N (RITA Project). *Oceanol. Acta*. (Spec. vol., "Geology of Oceans," 26 Congrès Geologique International, Paris, 1980), pp. 15–24.

Reynold, R. C., Jr., and Hower, J., 1970. The nature of interlayering in mixed-layer illite-montmorillonites. *Clays Clay Miner.*, 18: 25–36.

Rise Project Group, 1980. East Pacific Rise: Hot Springs and Geophysical Experiments. *Science*, 207(4438):1421–1433.

Robinson, P. T., Flower, M. J. F., Schminke, H. U., et al., 1977. Low temperature alteration of oceanic basalt, DSDP Leg 37. *In* Aumento, F., Melson, W. G., et al., *Init. Repts. DSDP*, 37: Washington (U.S. Govt. Printing Office), 775–789.

Scott, R. B., and Hajash, A. J. R., 1976. Initial submarine alteration of basaltic pillow lavas: a microprobe study. *Am. J. Sci.*, 276: 480–501.

Seyfried, W. E., Jr., and Bischoff, J. L., 1979. Low temperature basalt alteration by seawater: An experimental study at 70°C and 150°C. *Geochim. Cosmochim. Acta*, 43:1937–1947.

Seyfried, W. E., Shanks, W. C., and Bischoff, J. L., 1976. Alteration and vein formation in Site 321 basalts. *In* Yeats, R. S., Hart, S. R., et al., *Init. Repts. DSDP*, 34: Washington (U.S. Govt. Printing Office), 385–392.

van Andel, Tj. H., and Ballard, R. D., 1979. The Galapagos Rift at 86°W 2. Volcanism, structure and evolution of the Rift Valley. *J. Geophys. Res.*, 84(810):5390–5406.

Weaver, C. E., and Pollard, L. D., 1973. The Chemistry of Clay Minerals. *Dev. Sedimentol.*, 15: (Elsevier).

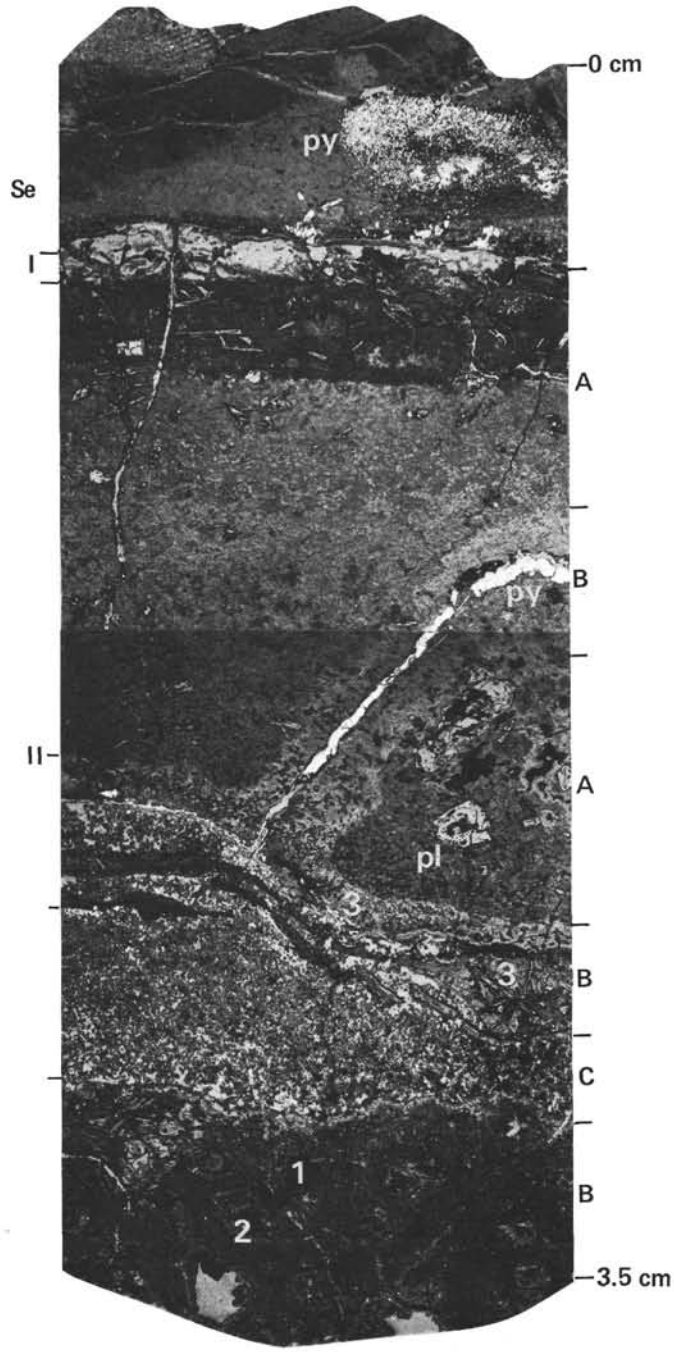

Plate 1. Basalt thin section showing the principal characteristic macroscopic features of an altered cooling unit margin (Sample 485A-38-2, 2–3). (Se = Indurated sediment in contact with basalt. I = Variolitic glassy zone in a matrix of yellowish-brown, beige, or greenish palagonitized glass. II = Microlitic zone. A—Homogeneous, more or less altered interstitial glass; basalt unfractured to only slightly fractured. B—Heterogeneous, strongly altered glass in highly fractured basalt. The glass has devitrified to form (1) concentric rims, (2) alternating layers, and (3) granular aggregates of palagonite and microcrystalline zeolites. C—Altered hyaloclastic breccia in a calcite cement along a fracture. Py = pyrite, in patches in the sediment and filling a vein in the microlitic zone. Pl = plagioclase phenocryst.)

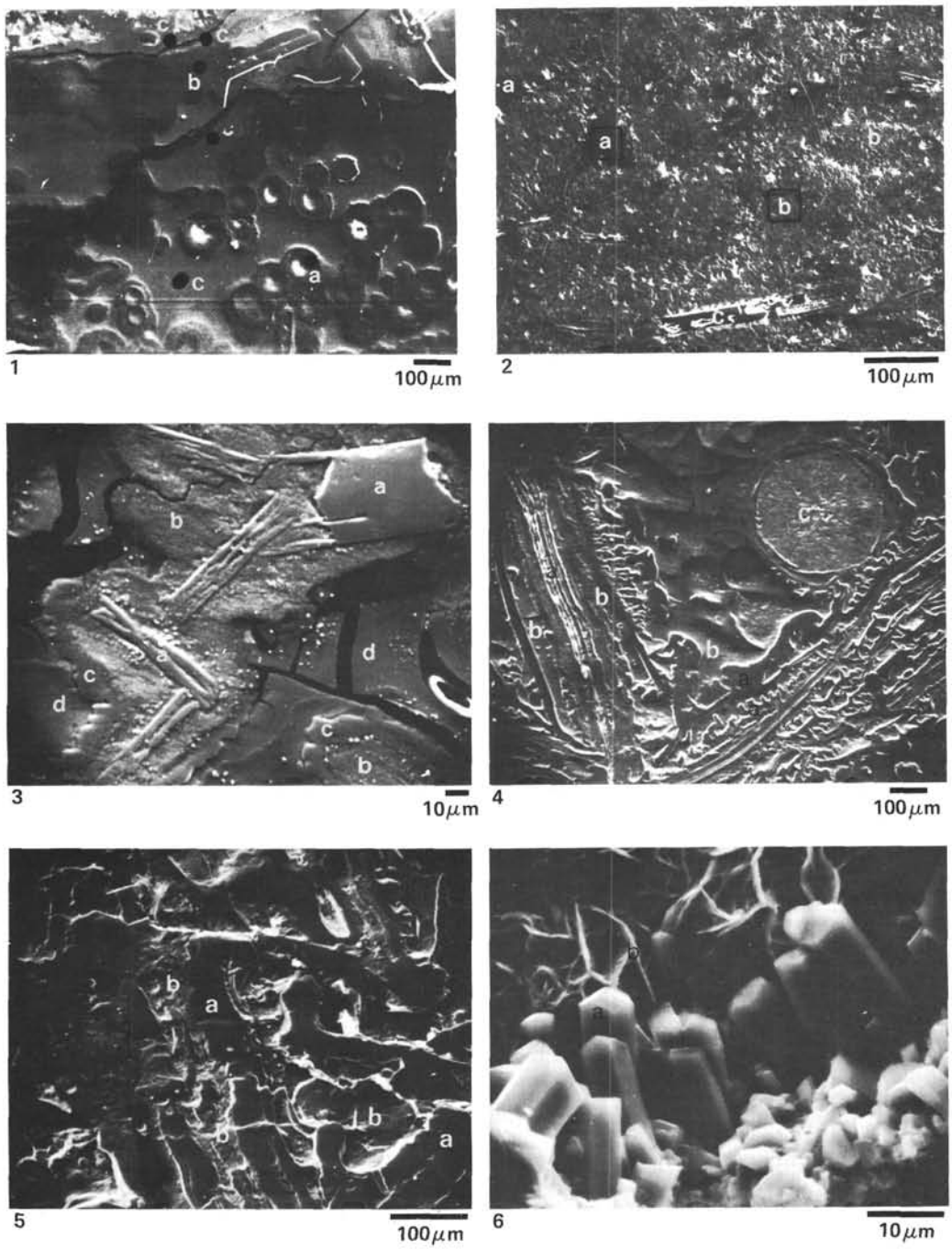

Plate 2. Photomicrographs of features shown in Plate 1. 1. Zone I: (a) isolated varioles of altered, potassium-rich glass, (b) coalescing varioles, (c) palagonite. 2. Zone II A: (a) fresh glass, (b) altered glass, (c) plagioclase microlite. 3. Zone II B(1): Central part of a polygonal hyaloclastic fragment showing (a) microlites of plagioclase, (b) surrounded by altered glass, (c) zeolite-rich glass, and (d) palagonitized glass. 4. Zone II B(2): Sub-parallel layers of (a) zeolite-rich glass and (b) palagonitized glass along microcracks; (c) Vesicle filled with clay minerals. 5. Zone II B(3): Fractured margin of a calcite-filled vein showing (a) zeolite-rich concretions (b) developed in altered glass. 6. Zone IIC: Altered fragment of hyaloclastic breccia showing vesicle filled with (a) zeolites (Na-Ca chabazite) and (b) clay minerals (mixed-layer chlorite-smectite).

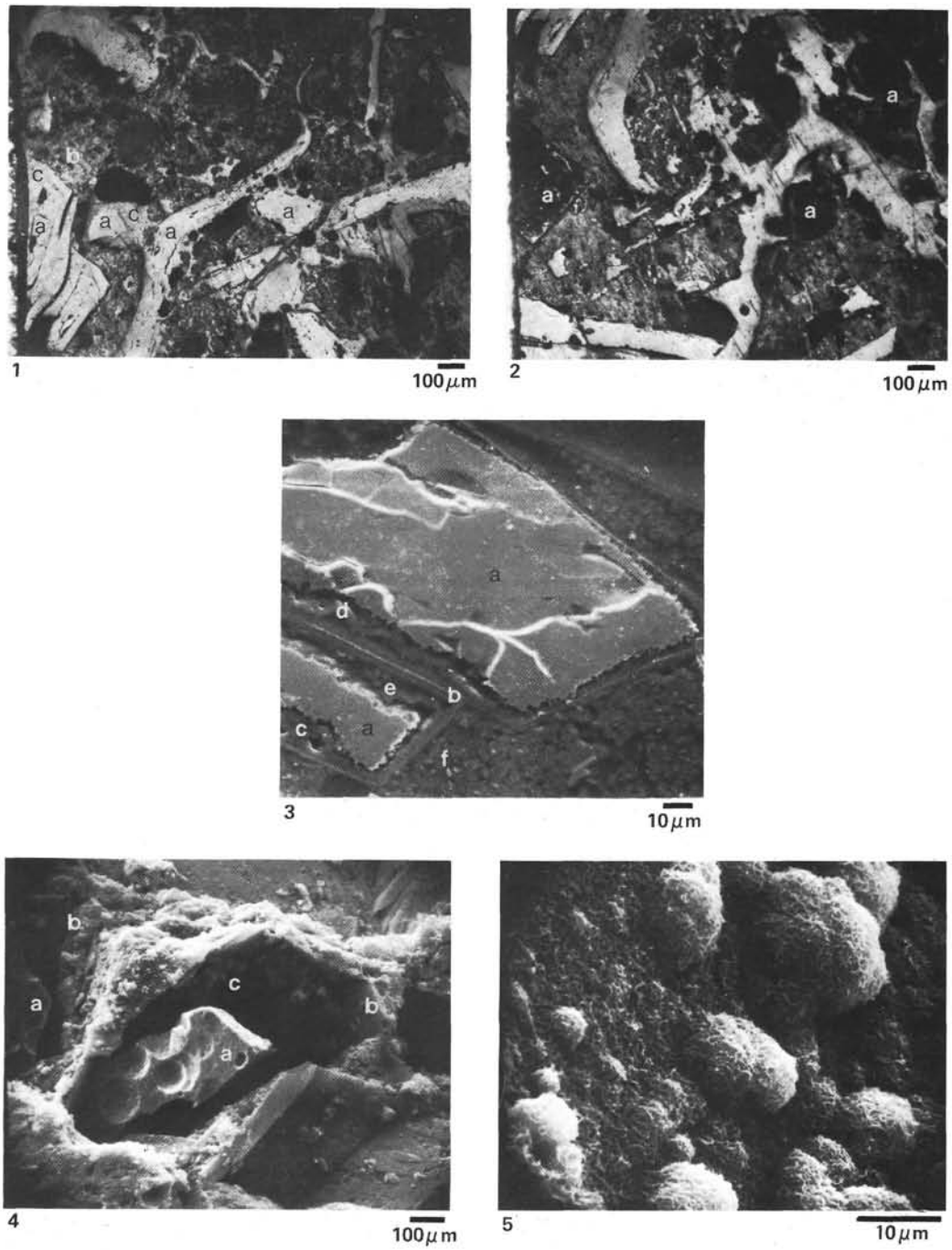

Plate 3. Characteristic microscopic features of a hyaloclastite-rich sediment (Sample 483-8-1, 59–65). 1. (a) Photomicrograph of glass shards and lamellae (b) in a groundmass of detrital clay minerals. (c) Cavities filled with resin for polishing process. 2. Photomicrograph of glass fragments completely altered and replaced by clay minerals showing (a) a more or less fine "pellet" texture. 3. Details of the alteration in glass fragments: (a) unaltered core; (b) palagonitized rim with a preserved massive texture; (c) altered glass, (d) progressively transformed into secondary clay minerals, and (e) exhibiting a micropellet texture; (f) detrital clay minerals. 4. SEM micrograph showing (a) preserved glass fragment in a cavity related to the original form of the fragment. The centripetal dissolution of the glass has not affected the (b) palagonitized glassy rim coating the inside cavity. (c) Scarce pellets fill the interstitial space between the fresh glass and its palagonitized rim. 5. Magnification of clay mineral "pellets."

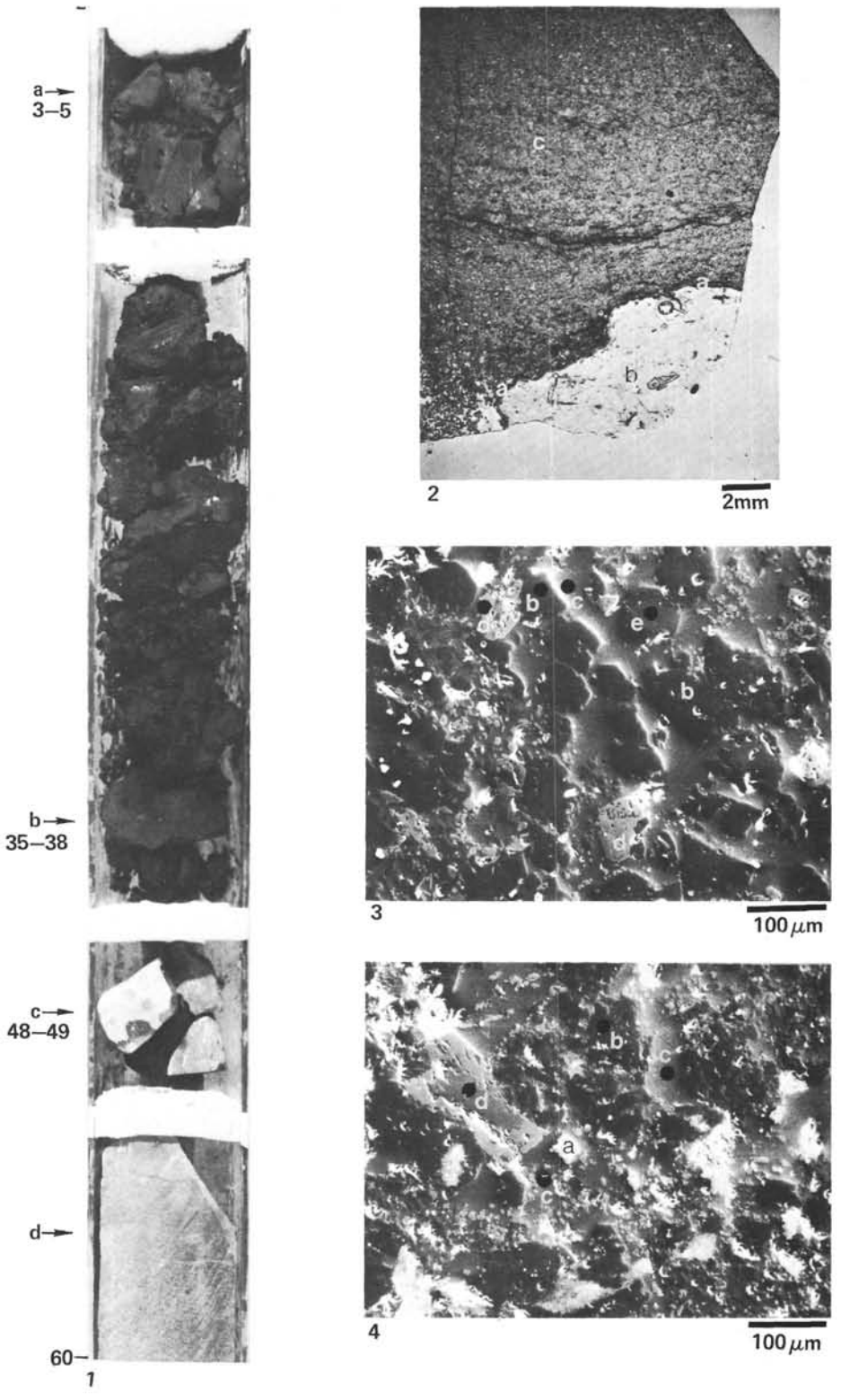

Plate 4. Characteristic macroscopic and microscopic features of sediments in contact with basalt (Section 485A-23-1). 1. General view of Section 23-1. (a) Unaltered claystone, (b) claystone altered during diagenetic processes, (c) greenish calcareous sandstone, coating the (d) aphyric basalt. Intervals indicate locations of samples taken for analysis. 2. Magnification of Zone C in Figure 1 showing (a) the glassy rim of (b) a poorly altered basalt margin, and (c) coarse bedding in the overlying sediment. 3–4. Details of calcareous sandstone: (a) pyrite, (b) albite, (c) calcite cement, (d) zoned clinopyroxene (core: Mg > Fe; margin: Fe > Mg), (e) zoned plagioclase (core: Na–Ca; margin: Na).